Carcinoma and SV40-Transfected Normal Ovarian Surface Epithelial Cell Comparison by Nonphotochemical Hole Burning

R. J. Walsh,* T. Reinot,* J. M. Hayes,* K. R. Kalli,† L. C. Hartmann,‡ and G. J. Small*
*Ames Laboratory—USDOE and Department of Chemistry, Iowa State University, Ames, Iowa 50011; †Endocrine Research Unit, Department of Internal Medicine, and ‡Division of Medical Oncology, Department of Oncology, Mayo Clinic and Mayo Foundation, Rochester, Minnesota 55905

ABSTRACT Results are presented of nonphotochemical-hole-burning experiments on the mitochondrial specific dye rhodamine 800 incubated with two human ovarian surface epithelial cell lines: OSE(tsT)-14 normal cells and OV167 carcinoma cells. This dye is selective for the plasma and inner membranes of the mitochondria, as shown by confocal microscopy images. Dispersive hole-growth kinetics of zero-phonon holes are analyzed with theoretical fits, indicating that subcellular structural heterogeneity of the carcinoma cell line is lower relative to the analogous normal cell line. Broadening of holes in the presence of an applied electric field (Stark effect) was used to determine the permanent dipole moment change for the $S_0 \rightarrow S_1$ transition in the two cell lines. For the carcinoma cell line, the permanent dipole moment change value is a factor of 1.5 higher than for the normal cell line. It is speculated that this difference may be related to differences in mitochondrial membrane potentials in the two cell lines.

INTRODUCTION

In proof-of-principle experiments in this group, it has been shown that hole-burning imaging (HBI) of a probe molecule is a viable technique for the identification of cellular anomalies (Milanovich et al., 1998a,b). HBI is a spectral hole-burning method that uses selective excitation to negate the effects of inhomogeneous broadening caused by the disordered (glass-like) nature of biological media and thereby images differences in selected cellular components. The particular spectral selection method used in HBI is nonphotochemical hole burning (NPHB), the mechanism for which is dependent on structural disorder (vide infra). As NPHB is highly sensitive to the molecular level details of the environment of a probe molecule, it is well suited to detecting subtle differences in subcellular components due to cellular dysfunction. NPHB has been widely used for investigating a variety of phenomena from spectral dynamics in glasses and polymers (Van den Berg and Völker, 1988; Reinot et al., 1997a,b; 1999; Silbey et al., 1996; Walsh et al., 1987; Hayes et al., 1999; Kador et al., 1987b), to the elucidation of electron and excitation energy transfer processes in photosynthetic reaction centers and antenna complexes (Reddy et al., 1993; Rätsep et al., 1998a,b, 2000; Wu et al., 2000; Zazubovich et al., 2002).

The mechanism of NPHB has been elaborated in a series of papers by Small and co-workers (Hayes and Small, 1978; Shu and Small, 1992; Reinot and Small, 2001) and has been discussed in several reviews (Jankowiak et al., 1993; Reinot et al., 2000, 2001). The reader is referred to those papers for further details. Here it suffices to note that in disordered solids at low temperatures, there are molecular groups which can occupy two (or more) nearly isoenergetic configurations separated by a potential energy barrier. These two-level systems (TLS) can be subdivided into those intrinsic to the disordered solid, intrinsic TLS (TLS_{int}), and those which are due to the presence of the dye molecule, extrinsic TLS (TLS_{ext}). Hole burning occurs via phonon-assisted tunneling of TLS_{ext} coupled to the dye molecule in its excited state. The tunneling occurs with a rate, $R = \Omega \exp(-2\lambda)$, where Ω is proportional to the square of the tunneling frequency, and λ is the tunneling parameter. As described by Shu and Small (1992), an outside-in process is involved where tunneling of the more distant TLS_{int} precedes the rate-determining step of tunneling of TLS_{ext}. It is the tunneling of TLS_{ext} which results in a shift of the absorption energy of the dye and, thus, a hole. This hole will persist as long as the sample lacks sufficient thermal energy for the reversion to the original molecular configuration.

In Milanovich et al. (1998a,b), an analogy was drawn between HBI and magnetic resonance imaging. This analogy was based on the fact that magnetic resonance imaging measures proton T_1 relaxation times, whereas HBI, in part, depends upon the T_2 optical dephasing time. That measurement of T_2 might be useful in detecting cellular/tissue anomaly was suggested by the work of Furusawa et al. (1994) on variation of photon echo decay of animal and human tissue samples stained with various rhodamine dyes. However, in Milanovich et al. (1998a), it was shown that hole width measurements for cells stained with the phthalocyanine dye, aluminum phthalocyanine tetrasulfonate (APT), could not be used to differentiate between a cell line derived from cancerous tissue and a related, nondiseased line. The hole width is the hole-burning parameter most directly dependent on T_2. However, one of the strengths of hole

Submitted July 31, 2002, and accepted for publication October 11, 2002.
Address reprint requests to Gerald J. Small, Ames Laboratory—USDOE and Dept. of Chemistry, 757 Gilman Hall, Iowa State University, Ames, IA 50011. Tel.: 515-294-3859; Fax: 515-294-1699; E-mail: gsmall@ameslab.gov.

0006-3495/03/02/1299/09 $2.00

burning is that there are a variety of parameters that can be measured and Milanovich et al. (1998a) showed that the cell lines did differ in their response to an applied electrical field.

In Milanovich et al. (1998a,b), the cells studied were from the cell lines MCF7 and MCF10F. These are human breast epithelial cells that are, respectively, a carcinoma cell line and a noncancerous line from the same patient. Each line was stained with the APT dye and hole-burning measurements made. Although no differences between the two cell lines were detected for hole widths, burn kinetics, or pressure shifts of holes, a small difference in the dipole moment change was measured by electric field effects (Stark effect). The failure to detect differences in other hole-burning parameters was attributed to the fact that the dye used was not organelle-specific, and the staining times used caused the dye to permeate throughout the cell. In the present work, a dye specific for the mitochondrial membranes is used. This organelle was targeted because it is known that there are significant differences in the membrane potentials of mitochondria in cancerous and normal cells.

In addition to changing the dye, different cells lines from those used previously were used. The reason for this was that the MCF-10F cell line, although originally derived from normal breast epithelial tissue, has become immortalized. From this it can be inferred that the cell line is no longer ''normal,'' as normal human cells do not propagate eternally. Fortunately, techniques utilizing expression of viral proteins such as the SV40 large T antigen, a protein that does not induce transformation or immortalization, have been developed to allow extended culture of normal cells (Maines-Bandiera et al., 1992; Nitta et al., 2001; Chou, 1989; Jenkins, 1999). These techniques have allowed the development of cell lines that can serve as appropriate controls for experiments on diseased cells.

In this work, new cell lines were chosen that would present improved comparative carcinoma and normal analogs, both of which are characterized and in the case of the normal analogs have not undergone immortalization. The means by which the latter was accomplished was to use the common technique of infecting the cells with a retroviral construct encoding a temperature-sensitive mutant of the SV40 large T antigen. This work extends the previous observations by using two epithelial ovarian cell lines: one, a carcinoma cell line derived from a high-stage, high-grade serous tumor, the most commonly diagnosed form of ovarian cancer, and the second, a line derived from normal ovarian surface epithelium (Conover et al., 1998). The studies on the normal line are possible because the cells express a temperature-sensitive large T antigen that allows growth of the cells at the permissive temperature (34°C). At the nonpermissive temperature (39°C), the mutant large T antigen is unstable and the protein is incapable of interacting with cell cycle control proteins to promote proliferation, leading to a halt in cell division and a return to baseline conditions (Resnick-Silverman et al., 1991). It is documented (Jha et al., 1998) that this method allows the cells to proliferate without the disadvantage of causing large genetic and/or morphological changes in the cells typically brought about by increased passaging of cell cultures obtained from normal tissue.

The cell lines utilized were of human ovarian surface epithelial origin, with the carcinoma cell line (OV167) having been characterized previously by Conover et al. (1998) and the temperature-sensitive SV40 normal analogs (OSE(tsT)-14) characterized by Kalli et al. (2002). Ovarian surface epithelial cells are thought to be involved heavily in the onset of ovarian cancer, as it has been documented (Scully, 1977) that ~90% of ovarian cancers have their origin in this cell type.

Here results of confocal microscopy are presented which verify the location of the MF680 dye within the mitochondria. Hole-burning results for the dye in the two cell lines are then presented which show that although hole widths and mean phonon frequencies of sideband holes are quite similar for the cell lines, the cell lines can be distinguished by hole-growth kinetics (HGK) or Stark broadening measurements. The HGK results are particularly interesting as these measurements could be made with an inexpensive diode laser and, thereby, may be useful for screening of cell populations. The Stark measurements, on the other hand, are more involved, but may be a useful technique for investigating mitochondria and mitochondria membrane potential. In the present study, the permanent dipole moment changes of the cell lines as determined by the Stark measurements differ by a factor of 1.5 for the two cell lines. This difference is similar to the difference of mitochondrial membrane potential between cancerous and normal cell lines (Johnson et al., 1980; Summerhayes et al., 1982; Modica-Napolitano and Aprille, 1987; Davis et al., 1985; Dairkee and Hackett, 1991).

EXPERIMENTAL

Cell culture

Two lines of Ovarian Surface Epithelial Cells were cultured for the model cell lines: OV167 (cancerous) and short-term normal ovarian surface epithelial (OSE) cell cultures infected with pZipSVtsA58, a retrovirus encoding a temperature-sensitive mutant of the SV40 large T antigen. For simplicity, we will refer to the latter as OSE(tsT)-14. OV167 cells were cultured in Alpha MEM with nucleosides (Irvine Scientific; Santa Ana, CA), supplemented with 20% Fetal Bovine Serum, Penicillin/Streptomycin (100 U/ml and 100 μg/ml, respectively), and L-Glutamine (2 mM final concentration, resupplemented every 2 weeks). OSE(tsT)-14 cells were cultured in a 1:1 mixture of Medium 199 and MCDB105 medium, supplemented with 15% Fetal Bovine Serum, Penicillin/Streptomycin (100 U/ml and 100 μg/ml, respectively), and L-Glutamine (2 mM final concentration, resupplemented every 2 weeks). Both cell lines were cultured to subconfluent populations, harvested, and then cryopreserved in 1-mL aliquots with 5% Dimethyl Sulfoxide (DMSO). For each hole-burning experiment, an aliquot of cells was cultured for 6–7 days (nonconfluent samples) or 12 days (confluent samples) before staining and cryopreservation. OV167 cells were grown at 37°C and 5% CO_2 atmosphere. OSE(tsT)-14 cells were grown at the permissive temperature of 34°C, 5% CO_2 for

SV40 Large T antigen. For cells in which it was desirable to keep the antigen present (ltOSE(tsT)-14), cells were stained and cryopreserved at the desired coverage conditions. For cells in which the SV40 Large T antigen was desired to be denatured (htOSE(tsT)-14), cells were cultured to desired coverage conditions and subsequently incubated for 12–18 h at 39°C and 5% CO_2 before staining and cryopreservation. Unless otherwise noted, all chemicals were purchased from Sigma-Aldrich (St. Louis, MO).

Staining

Staining of the culture was accomplished by dissolving the MF680 (rhodamine 800; MitoFluor Far Red 680, Molecular Probes, Eugene, OR) initially in DMSO, then diluting into 1× Phosphate Buffered Saline to the desired concentration for staining. Incubations were carried out under normal culture growth conditions, and cells were rinsed three times with Phosphate Buffered Saline before cryopreservation. Hole-burning experiments were conducted with cells stained with MF680 at a concentration of 40 nM for 15 min; confocal experiments were conducted as noted.

Cryopreservation

Cells were cryopreserved by suspending in 130 μL of their respective medium with 5% DMSO and subsequent placement in a gelatin capsule. Because the capsules tended to soften and dissolve before freezing, two sizes were used (#4 and #5), with the smaller #5 being placed inside the larger #4. The entire suspension was placed in a Nalgene Cryo 1°C freezing container (Nalgene Products; Rochester, NY) and frozen to −70°C undisturbed for at least 4 h. Capsules were then plunged directly into liquid helium for hole-burning studies. Cells were also tested for poststaining and freezing viability by rapidly thawing and returning the cells to their respective medium.

Confocal microscopy

All confocal and time-lapse imaging was performed at the Roy J. Carver Laboratory for Ultra-high Resolution Biological Microscopy (Iowa State University; Ames, IA). The microscope utilized for both imaging methods was a Nikon Eclipse TE200 with an inverted 60× oil-immersion lens (NA: 1.40; Theoretical Resolution at 632.8 nm: 0.276 μm). The confocal/video instrumentation was manufactured by Prairie Technologies, LLC (Middleton, WI). Confocal imaging was performed with He-Ne (632.8 nm) and Ar^+ (514 nm) ion lasers for excitation, with photomultiplier tube (PMT) detection, and a pinhole size set to 100 μm. All software to control the hardware was by Prairie Technologies utilizing National Instruments LabView 5.1.

Cells were grown and imaged on poly-L-Lysine (Sigma; St. Louis, MO) treated coverglass (25 × 75 mm). To facilitate multiple stainings without removing the sample from the microscope, an in-house silicone culture well (vol. ~0.5 mL) was created and affixed to the glass. Cultures were transferred 24–48 h before use, and were incubated under normal conditions. All images were collected within 1 h of preparation. Cells cultured for use in confocal microscopy studies were not passage-restrained, but were within one passage of those used for hole-burning studies.

Laser/cryostat system for hole burning

The fluorescence excitation system has been previously described (Milanovich et al., 1998b), with the exception of a few modifications. In brief, a ring dye laser using LD 688 (Exciton; Dayton, OH) was pumped by a Coherent Innova 90-6 argon ion laser (Coherent; Santa Clara, CA). The laser system provided 100–500 mW power over a wavelength region of 660–720 nm. Laser intensity was stabilized by an LS100 laser power stabilizer (Cambridge Research and Instrumentation; Cambridge, MA) and the laser beam spot was expanded with a telescope. Two scanning modes were utilized: broad-range scanning without intercavity etalons (scanning range and linewidth of 1000 cm^{-1} and 0.1 cm^{-1}, respectively) and short-range scanning with intercavity etalons (scanning range and linewidth <1.5 cm^{-1} and <0.0003 cm^{-1} (<10 MHz), respectively). When necessary, laser polarization was controlled with a polarization rotator.

Laser intensity for hole burning and scanning was varied with the use of a series of neutral density absorption filters. Scanning fluences were chosen to avoid additional burning during the scan. Burn kinetics were collected with rapid sampling at 0.1 s per channel for the first 30 s, as the signal tends to show the greatest decrease in this time. After 30 s, channel collection time was increased to 1 s.

Fluorescence intensity was measured with a Hamamatsu model R2949 multialkali PMT and photon counter (Model #SR-400, Stanford Research; Sunnyvale, CA). A 720-nm low pass filter (Model #720ALP, Omega Optical; Brattleboro, VT) was used to block excitation frequencies from reaching the PMT. Laser scanning and data collection were done with a computer running in-house software.

For the cells and the glycerol-water mixture, hole burning was performed with the sample mounted in a continuous flow cryostat (Model STVP-100, Janis Research; Wilmington, MA). Both kinetics and Stark experiments were done using a sample holder described previously (Milanovich et al., 1998a). Briefly, for the Stark experiments two Teflon walls separated by 11 mm and positioned parallel to the cryostat walls hold two copper electrodes positioned perpendicular to the cryostat walls and separated by 4.95 mm. The hole-burning apparatus for the hyperquenched glassy water (HGW) system has been described previously (Reinot and Small, 2001), and was performed by thermospraying an aqueous MF680 (10^{-5} M) solution onto a copper block under vacuum and at ~5 K.

RESULTS

Confocal and microscope studies

Confocal microscopy images of the two cell lines OV167 and OSE(tsT)-14 are presented in Fig. 1. A noteworthy feature of the images for the OV167cells in Fig.1 *B* and the OSE(tsT)-14 cells in Fig.1 *D* is the observation of the dye in a specific, structured organelle, which most closely resembles mitochondria when referenced to other studies staining for in situ mitochondria (Chen et al., 1982). To rule out the possibility that the MF680 dye was locating preferentially elsewhere than the mitochondria in either cell line, two tests were conducted. The first was to add a small amount of sodium azide to the culture while imaging on the microscope; within several seconds, the fluorescence intensity of the cells was observed to diminish (data not presented). Sodium azide is a toxin targeted to enzyme complex IV in the mitochondria electron transport chain, resulting in deterioration of the mitochondrial membrane potential. Inasmuch as the MF680 dye is cationic and requires the membrane potential to maintain its position within mitochondrial membranes, this observation was the direct result of the MF680 being released by the mitochondria to levels below detection due to the insult by the sodium azide. The second test conducted was to target and stain the endoplasmic reticulum, suspected as a possible alternative repository for the MF680 molecule due to similarities to mitochondria in maintaining a membrane potential and having a lipid structure. This was accomplished by using a second dye, Molecular Probes' BODIPY conjugated to Brefeldin-A (with a noninterfering absorbance and

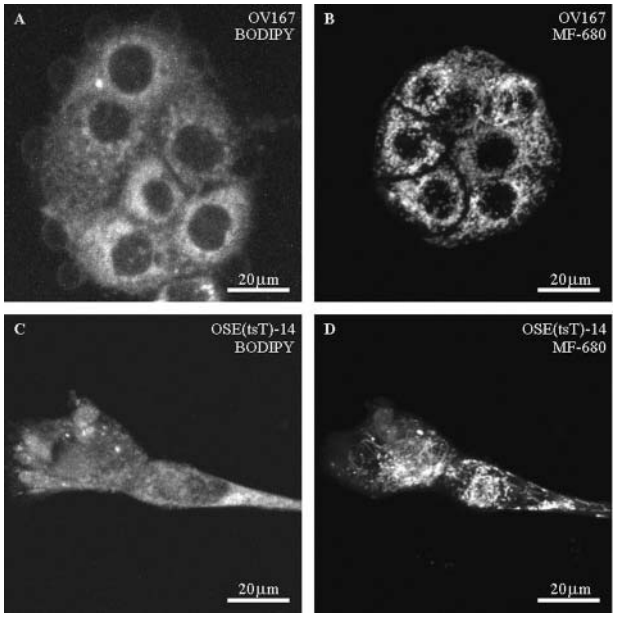

FIGURE 1 Confocal images of OV167 (carcinoma) cells (*A, B*) and OSE(tsT)-14 (normal analog) cells (*C, D*). Images in *A* and *C* were stained with Brefeldin-A BODIPY, specific for the endoplasmic reticulum. Images in *B* and *D* were stained with MF680, specific for mitochondria. The white bar represents 20 μm.

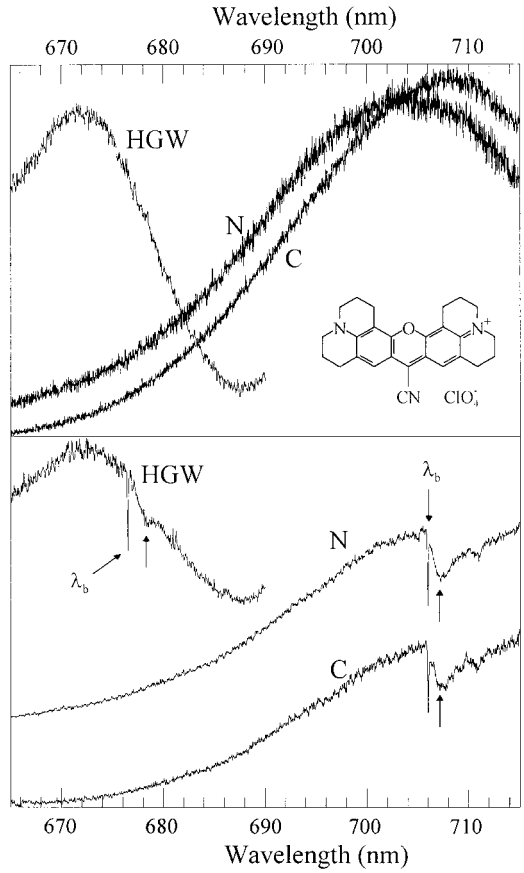

FIGURE 2 (*Top*) Fluorescence excitation spectra of MF680 in hyperquenched glassy water (HGW), OSE(tsT)-14 normal cells (*N*), and OV167 carcinoma cells (*C*). The inset is the structure of the dye molecule, MF680. (*Bottom*) Post-burn spectra, exhibiting the ZPH and the pseudo-phonon side band (PSB) for each type of sample. Fluences for the cellular samples are 33 mJ/cm^2 and for HGW, 1.4 J/cm^2. The burn wavelengths, λ_b, are labeled. Displaced to longer wavelength from the ZPH coincident with λ_b are the pseudo-phonon sideband holes, indicated by upward-pointing arrows.

fluorescence relative to MF680), added to a culture in growth medium and mounted on the microscope. After a short incubation and collection of confocal images where the BODIPY dye is the source of the fluorescence signal, MF680 was added and subsequently allowed to incubate for a short period and then imaged. The results are presented in Fig. 1, *A* and *C*, where the two cell lines are presented for comparison. It is apparent from an inspection of the structures stained by each dye that their positions and morphology differ, and hence provides further evidence of MF680's preference for mitochondrial membranes.

Dispersive hole-growth kinetics of MF680

Fig. 2 exhibits fluorescence excitation spectra for three types of samples, one formed by hyperquenching a solution of MF680 dissolved in water and two samples with intracellular MF680. The HGW sample was prepared for a preliminary investigation of MF680 to determine hole-burning properties of the dye. Fig. 2 *A* presents the fluorescence excitation spectra before hole burning whereas Fig. 2 *B* shows the spectra after laser excitation with the fluences given in the figure caption and at the burn wavelength, λ_B, indicated in the figure. The spectra shown in Fig. 2 *B* are typical: a sharp hole coincident with the burn wavelength (the zero-phonon hole, ZPH) and to longer wavelength a broad hole due to burning of sites which absorb at λ_B through phonon absorption (the pseudo-phonon sideband hole, pseudo-PSBH). Both the ZPH width and the pseudo-PSBH frequency displacement from λ_B are characteristic of the hole-burning system (dye plus matrix). In the present case, however, there is no significant difference between these parameters for the two cell lines (vide infra). Other characteristic hole-burning parameters which can be measured are the rate of growth of the ZPH and its broadening or splitting with an applied electric field or with applied pressure. Hole-growth kinetics are presented in this section and electric field-induced broadening data in the next section. Pressure broadening measurements were not a part of the present study.

Before proceeding to discuss the HGK results, the fluorescence excitation spectra and the static hole properties are remarked upon. Noteworthy from Fig. 2 *A* is that there is a large red shift in the MF680 in vivo excitation maximum relative to the HGW sample, with the OV167 carcinoma (*C*) cell line being further red-shifted than the OSE(tsT)-14 normal (*N*) cells by ~3 nm. Shown in Fig. 2 *B* are representative ''deep'' burns, created with fluences for the intracellular samples of 1.4 J/cm^2 and for the HGW sample, 33

mJ/cm^2. The sharp feature coincident with λ_B is the zero-phonon hole. To lower energy of the ZPH are pseudo-phonon sideband holes (marked with *arrows* in the figure). For the HGW and normal cells the PSBH is observed to be 30 ± 3 cm^{-1} and for the carcinoma cells 28 ± 3 cm^{-1}. Although not significantly different between the two cell lines, the large separation between the ZPH and the PSBH translates into favorable conditions for observing HGK for the formation of ZPHs with little or no interference from the PSBH.

A representative comparison of the burn kinetics for each of the two cell lines is presented in Fig. 3. Fits (vide infra) obtained from the data are superimposed to show the agreement with actual data. It is apparent from the figure that the carcinoma cells burn to a deeper fractional hole depth with respect to the normal cells in the same amount of time for the same burn intensity. Experimentally obtained NPHB kinetics curves were fit using (Reinot and Small, 2000):

$$D(t) = \int d\lambda f(\lambda) \int d\alpha \sin\alpha \cos^2\alpha e^{-P\sigma_{LT}^{p}\phi(\lambda)\cos^2(\alpha)t}, \quad (1)$$

where $1 - D(t)$ is the fractional hole depth following a burn for time t at a burn frequency ω_B. P is the total photon flux with units of number of photons cm^{-2} s^{-1}. P was determined from the laser power, taking into consideration the beam size at the sample and attenuating filters in the beam path. α is the angle between the laser polarization and the molecular transition dipole, and $f(\lambda)$ is the Gaussian distribution function of tunneling parameter λ for the TLS_{ext} active in hole burning. The unitless parameter λ_0 is the distribution center and σ_λ, the standard deviation of the distribution. The parameter σ_{LT}^{p} is the peak absorption cross-section (2.8×10^{-12} cm^2). The average quantum yield for hole burning, ϕ, is given by (Reinot et al., 1997b):

$$\phi(\lambda) = \frac{\Omega \exp(-2\lambda)}{\Omega \exp(-2\lambda) + \tau^{-1}} \approx \frac{\Omega \exp(-2\lambda)}{\tau^{-1}}, \quad (2)$$

where $\Omega \exp(-2\lambda)$ represents the phonon-assisted tunneling relaxation rate, with Ω set to 7.6×10^{12} s^{-1} (Kim et al., 1996) and τ, the fluorescence lifetime, was determined to be 1.8 ns in aqueous solution at 77 K. A quantum mechanical expression for Ω can be found in Kenney et al. (1990). Note that the parameters λ and α each cause a distribution of hole-burning rates that leads to dispersive kinetics, and it has been shown (Reinot and Small, 2000) that the λ distribution is the dominant factor for the first ~80% of the burn (to saturation). When fitting kinetics data, it is necessary to know the Huang-Rhys (S) factor. The maximum depth of the saturated ZPH is given by e^{-S}. For the fits shown, S was set equal to 1.1, based on independent measurements of saturated hole depths (data not shown). In the fitting procedure, the value of S determines the limiting value of $D(t)$. The data presented in Table 1 represent the average values of λ_0 and σ_λ from multiple experiments for each cell type. Fig. 4 compares the hole-growth kinetics for burn wavelengths that approximately account for the observed shift in fluorescence excitation profiles between cell types. By comparing burn wavelengths that are offset by ~2 nm (compared to the ~3-nm shift in fluorescence excitation maxima), the data are corrected for any burn wavelength dependence of the kinetics. The HGK curve for the normal cells was burned at 710 nm, and the carcinoma line was burned at 712 nm. As can be seen in the curves, burn rate differences are still observed for each cell line.

Application of stark fields

In the work of Milanovich et al. (1998a), differences between the hole-burning properties of MCF-7 and MCF-10F human breast epithelial cell lines were only observed for the Stark broadening data. Although the kinetics measurements presented above easily distinguish between the two ovarian cell

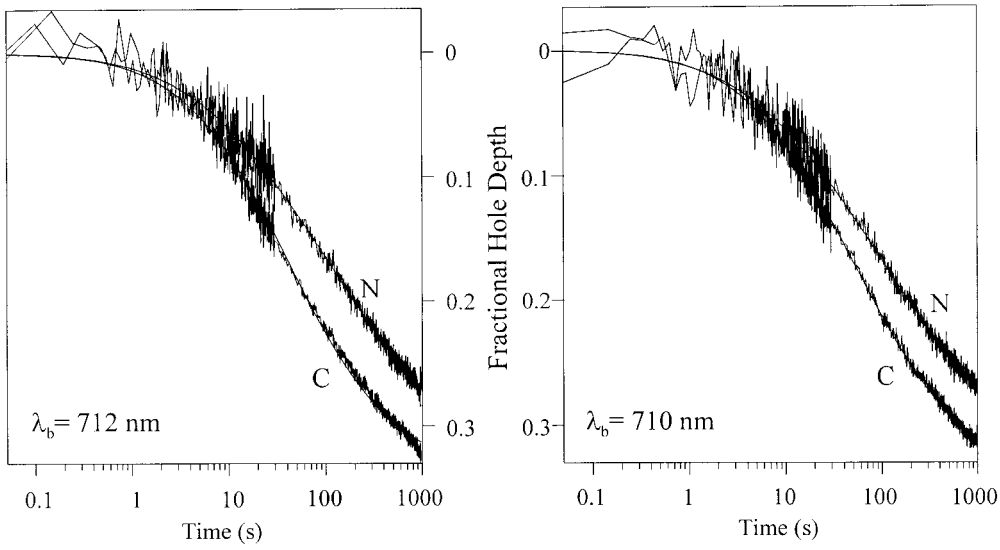

FIGURE 3 Representative hole-growth kinetics curves at 2 K for each cell type, with (*N*) the OSE(tsT)-14 normal cells and (*C*) the OV167 carcinoma cells. Smooth lines are fits using Eq. 1.

TABLE 1 Dispersive hole-growth kinetics fit parameters

λ_B (nm)	OV167 λ_0	OSE(tsT)-14 λ_0	OV167 σ_λ	OSE(tsT)-14 σ_λ
712	7.84 ± 0.10	8.36 ± 0.10	0.68 ± 0.10	1.15 ± 0.08
710	7.78 ± 0.13	8.36 ± 0.12	0.85 ± 0.10	1.10 ± 0.09
707	7.80 ± 0.11	8.41 ± 0.10	1.07 ± 0.10	1.19 ± 0.08
705	7.76 ± 0.12	8.61 ± 0.12	1.05 ± 0.10	1.22 ± 0.10

lines of interest here, Stark measurements were made to compare with the results of Milanovich et al. (1998a).

Representative results for the application of external electric fields ($\mathbf{E}_{St}$) to MF680 in a water-glycerol mixture (1:1) and in OV167 cells are presented in Fig. 5. Note that the signal-to-noise ratio is lower for the dye in mitochondria than for the dye in aqueous solution. This is due to a reduction in fluorescence quantum efficiency of ~4 as has been reported previously by others (Sakanoue et al., 1997). Despite the lower signal to noise, data over a sufficient range of voltages can still be obtained. Data for only one of the cell lines is displayed. Superimposed on the ZPH profiles are Lorentzian fits.

Stark hole-burning results are usually analyzed using the theory of Kador et al. (1987a). This is a rigorous theory which has been successfully used to understand a wide variety of hole-burning systems (see e.g., Wu et al., 2000; Rätsep et al., 1998a,b). Using the Kador theory and the ZPH fits, full widths at half maximum of the ZPH (Γ) are plotted against $\mathbf{E}_{St}$ according to the following equation:

$$\Gamma(F) = \gamma(1 + F^2)^{1/2}, \tag{3}$$

where γ is the width of the ZPH at zero field and includes contributions from both the homogeneous width of the ZPH plus any additional width from spectral diffusion or fluence broadening. F is defined by

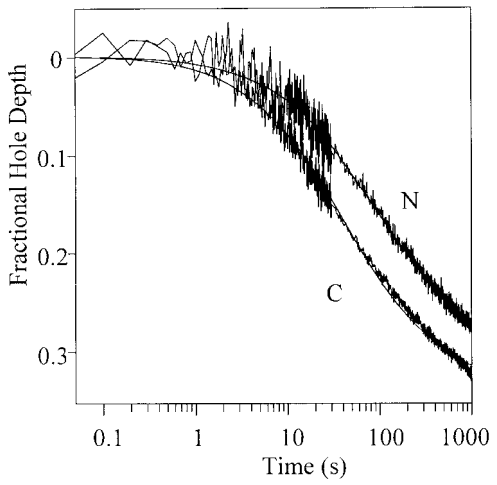

FIGURE 4 Hole-growth kinetics curves at 2 K for each cell type, with (*N*) the OSE(tsT)-14 normal cells and (*C*) the OV167 carcinoma cells. Smooth curves are fits to the data using Eq. 1. The curve for *C* was burned at 712 nm, and the curve for *N* was burned at 710 nm, to account for differences due to the fluorescence excitation shift observed between the two cell lines.

$$F = \frac{2f\,\Delta\boldsymbol{\mu}\mathbf{E}_{St}}{\hbar\gamma}. \tag{4}$$

The parameter f is the local field correction factor and is taken to be a scalar. Note that Eq. 3 was derived assuming that the variance of $\Delta\mu$ is zero. However, for $F \leq 3.5$, a condition met in the present work, use of a distribution for $\Delta\mu$ makes little difference. Eq. 3 provides a relation by which $\Delta\mu$, the change in permanent molecular dipole moment, can be determined from the ZPH width at an applied $\mathbf{E}_{St}$. This parameter can be written as $\Delta\mu = \Delta\mu_{mol} + \Delta\mu_{ind}$, where $\Delta\mu_{mol}$ is the intrinsic molecular dipole moment change and $\Delta\mu_{ind}$ is the matrix-induced dipole moment change. The relative magnitudes of these two terms determine whether Stark splitting or Stark broadening will be observed. If $\Delta\mu_{mol}$ is dominant, the photoselection phenomenon enables one to probe molecules for which the angle between $\Delta\mu_{mol}$ and the polarization vector of the light is well-defined. In this case a Stark splitting will be observed for one of the orientations of $\mathbf{E}_{St}$. However, when $\Delta\mu_{ind}$ is dominant only Stark broadening is observed because the orientations of $\Delta\mu_{ind}$ relative to the molecular transition dipole is random for a disordered matrix. In the present case, only broadening of holes is observed, indicating that $\Delta\mu_{ind} \gg \Delta\mu_{mol}$. Further discussions of the significance of dipole moment measurements with regard to cellular ultrastructure will be given later. In Fig. 6, the solid curves are representative theoretical fits using Eq. 3 illustrating the dependence of hole width on $\mathbf{E}_{St}$. Only the linear Stark effect is observed, which occurs when the internal electric field surrounding the chromophore is considered to be much larger than $\mathbf{E}_{St}$ (Rätsep et al., 1998a).

Measurements of $f\Delta\mu$ for MF680 in several types of samples are presented in Table 2. Contained within the table are some previously reported values for the sake of comparison. The $f\Delta\mu$ values for MF680 in a 1:1 mixture of water-glycerol are quite similar to those for the dye in OSE(tsT)-14 cells. For water-glycerol, only one polarization of the laser, $\mathbf{E}_L$, relative to $\mathbf{E}_{St}$ is presented (the parallel case), inasmuch as for $\mathbf{E}_L \perp \mathbf{E}_{St}$ Stark splitting was observed. Splitting was not observed in either cell line, however, a result of intercellular dye molecule orientations being random (vide infra). Notably, the $f\Delta\mu$ values presented here show roughly a 1.5-fold increase in the carcinoma cells over the normal analogs. OSE(tsT)-14 cells were also stained without high temperature incubation treatment to test for any effect the SV40 virus might have on the cell. The normal analogs with the SV40 antigen still present (ltOSE(tsT)-14) exhibit an intriguing result, in that the measured $\Delta\mu$ changes roughly align with those of the OV167 carcinoma line. This is explained considering the mechanism of SV40 transfection: the still-present antigen preferentially binds to the p53, pRb, and p300 proteins, all of which are involved in cell proliferation control (Ali and DeCaprio, 2001; Jha et al., 1998). Interestingly, OSE(tsT) cells are similar to normal

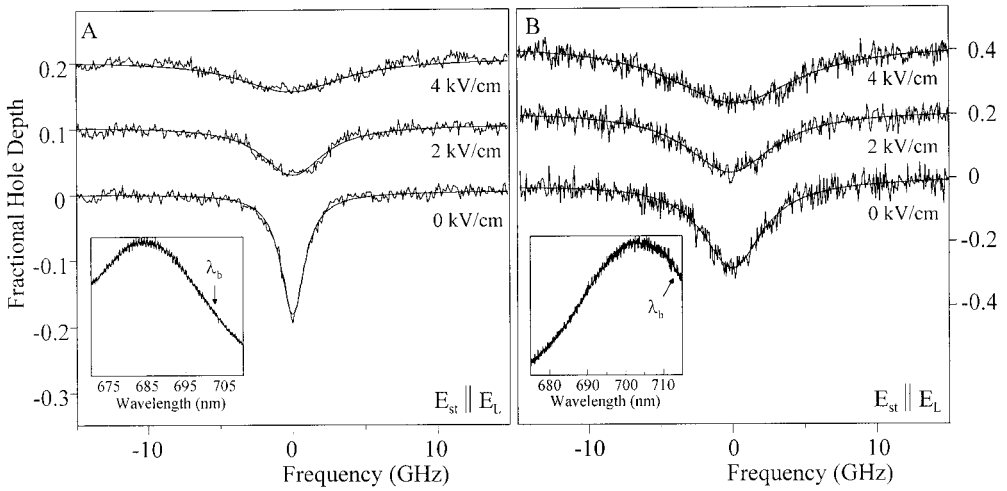

FIGURE 5 Representative Stark broadening curves at 2 K for MF680 in 1:1 water:glycerol (*A*) and in OSE(tsT)-14 normal cells (*B*). The inset in both *A* and *B* shows the fluorescence excitation profile and the burn location. Only parallel orientations of E_{St} to E_L are shown, as splitting occurred in the perpendicular orientation of *A* and the broadening for *B* was qualitatively similar to the parallel orientation.

OSE cultures at 39°C and more closely resemble malignant cells at 34°C in regulation of certain aspects of the insulin-like growth factor binding protein protease system, as well (K. R. Kalli, unpublished results).

DISCUSSION

Differences in the fluorescence excitation spectrum, hole-growth kinetics, and hole-burning Stark shifts are clearly seen in the data presented, demonstrating that NPHB has the capability to resolve differences between the cell lines used. The success of these findings is based in large part on the ability of the probe dye MF680 to locate specifically in in situ cellular mitochondria which are documented to have undergone ultrastructural alterations due to carcinogenesis.

From the data presented in Fig. 3, it is evident that the MF680 probe molecule is located in a nonaqueous environment. MF680 excitation profiles show a large red shift in the dye located in either cell line relative to the dye being located in water (HGW or a glycerol-water glass). The dye molecule is lipophilic and cationic, and thus preferentially locates in the lipid-based, negatively charged mitochondria. Although there is a shift in the fluorescence excitation profile between the two cell lines, the spectral shift is small relative to the profile width, and would not be accurate as a diagnostic due to uncertainties in measurements that would accompany large-scale sampling techniques. Furthermore, these shifts would not be evident in heterogeneous mixtures of samples, whereas hole-burning characterization has the potential for resolving differences in such samples (vide infra).

Interpretation of the above results concerning HGK provides intriguing insight into the cell line ultrastructures. Recalling that the λ-distribution is dominant in Eq. 1, fitting kinetics curves yields σ_λ, the standard deviation of the distribution, and, thus, a parameter that directly reflects the order of an amorphous matrix (structural heterogeneity). For the two cell lines presented, the carcinoma cells display lower values for λ_o (the mean distribution of tunneling rates) and σ_λ (distribution standard deviation). Notably, the σ_λ value is directly related to the degree of structural heterogeneity of a guest imbedded in a structurally disordered host, and in the present case is interpreted to mean that carcinoma mitochondrial ultrastructures are more ordered relative to

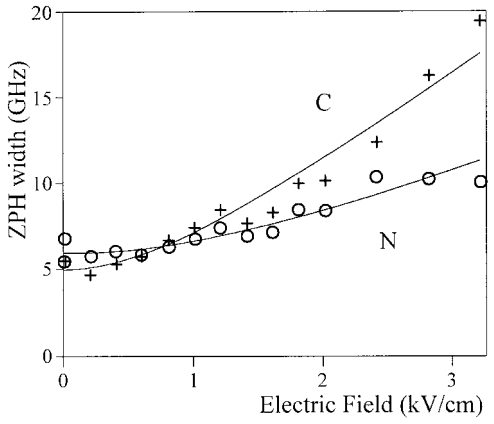

FIGURE 6 Fits of Stark broadening data to Eq. 3. *N* represents the OSE(tsT)-14 normal cell line, and *C* the OV167 carcinoma cell line.

TABLE 2 Permanent dipole moment changes for MF680 and APT in aqueous and in in vivo samples

Cell line	$f\Delta\mu$ (*D*)	Laser polarization	λ_b (nm)
htOSE(tsT)-14	1.64 ± 0.24*		711.8
OV167	2.47 ± 0.10*	$\mathbf{E}_{St} \perp \mathbf{E}_L$	711.8
ltOSE(tsT)-14	2.72 ± 0.20		711.8
htOSE(tsT)-14	1.68 ± 0.32*		711.6
OV167	2.51 ± 0.12*	$\mathbf{E}_{St} \parallel \mathbf{E}_L$	711.6
ltOSE(tsT)-14	2.86 ± 0.22		711.6
Water-glycerol	1.65 ± 0.05		704.0
MCF-7	0.20 ± 0.01†	$\mathbf{E}_{St} \parallel \mathbf{E}_L$	678.0
MCF-10F	0.27 ± 0.01†		677.5
MCF-7	0.21 ± 0.01†	$\mathbf{E}_{St} \perp \mathbf{E}_L$	677.5
MCF-10F	0.22 ± 0.01†		678.0

*Walsh et al., 2002
†Milanovich et al., 1998a

the normal cell line. Reasoning behind this observation in HGK differences is limited to speculation at this point, but may be due to structural differences noticed in confocal microscopy studies. From these studies, it was observed that the OV167 cell line exhibits small, more cobblestone-like shapes for the majority of the cells. Experiments were also conducted with higher magnification ($100\times$) than presented in Fig. 1 ($60\times$), with the further finding that the mitochondria observed within the OV167 cells are shorter, more highly aggregated structures relative to the OSE(tsT)-14 normal cells, possibly due to the rapid proliferation rate of the carcinoma cell line. It is conceivable that these smaller structures are more uniform in ultrastructure as a consequence of the increased rate of cellular reproduction, and this would dictate that long networks of mitochondria were not formed within the time frame used in these experiments. Such networks were observed in the normal cells, as with passage these cells change from the rounded ''cobblestone'' morphology to the ''atypical,'' fibroblast-like morphology as previously characterized (Auersperg and Maines-Bandiera, 1994).

A point of importance from this data is the consideration of the ease with which dispersive HGK can be measured. The only necessity is the measurement of fluorescence intensity (versus time) with application of a narrow band laser at cryogenic temperatures, which can be accomplished with an inexpensive diode laser. Further, detection methods could be varied as well, and work to develop a detection system based on optical microscopy (with CCD detection) is proceeding (Walsh, 2002), with potential for use in analysis of single cells, cell smears, and tissue samples. Other hole-burning parameters that were measured for the cell lines were ZPH width, mean-phonon frequency, and electron-phonon coupling strength. The ZPH widths and electron-phonon coupling strengths did not differ significantly for the two cell lines. The mean phonon frequencies appear to differ slightly (see Fig. 2), but the difference is within the experimental error of the measurement. Thus, none of these parameters provide a reliable method of differentiating the cell lines. Although the Stark results also show differences between the cell lines, these measurements are more involved than the HGK measurements. Thus, the Stark differences are less likely to be useful as a diagnostic technique.

A final point of consideration regarding HGK is the observation that the σ_λ values for the carcinoma cells show a measurable burn frequency dependence (Table 1) for fitting parameters whereas the normal cells do not. It is possible that this is due to differences in the fluorescence excitation profile peaks observed between the two types of cells. For the normal cells, all the burn wavelengths used are to the red of the fluorescence excitation peak. For the carcinoma cells, however, the shorter burn wavelengths are to the blue of the peak. Thus as the burn wavelength decreases for the carcinoma cells, there is more likelihood of vibronic hole burning that may interfere with the kinetics measurements.

The Stark values presented in Table 1 show further evidence of unique interactions between the MF680 dye and the surrounding cellular matrix for each cell line. Our previous interpretation (Walsh et al., 2002) of this data concluded that the 1.5-fold increase in permanent dipole moment changes for carcinoma cells were consistent with the observations of others (Johnson et al., 1980; Summerhayes et al., 1982; Modica-Napolitano and Aprille, 1987; Davis et al., 1985; Dairkee and Hackett, 1991) who have measured $\Delta\psi_m$ to be $\sim$1.5-fold higher in cancerous cells, and that this was the source of the increase for the $f\Delta\mu$ values determined. Experiments to measure $\Delta\psi_m$ for the cell lines used here are under way. Also hole-burning experiments are planned utilizing a dye probe specific for mitochondria that is not dependent on membrane potential for specificity.

For reference, Stark data from the MCF7 and MCF10F cell lines are also presented in Table 1. With these cell lines, it was speculated that the slight difference seen in the dipole moment changes between the MCF10F and MCF7 line for the case of $\mathbf{E}_{St} \parallel \mathbf{E}_L$ was attributable to $\Delta\mu_{ind}$ not being completely random, and that some degree of ordering existed within the MCF10F cells that did not exist within the cancer cells. For the present case, however, neither orientation of $\mathbf{E}_{St}$ with $\mathbf{E}_L$ dominates, indicating that $\Delta\mu_{ind}$ dominates $\Delta\mu_{mol}$ and varies in sense from molecule to molecule.

An $f\Delta\mu$ comparison between the htOSE(tsT)-14 and that of water-glycerol exhibits no difference within experimental uncertainty. These cells were found to be viable after freezing, staining, and resuspending in growth medium, and also exhibited the large fluorescence excitation profile red shift relative to MF680 in water-glycerol, so that cell death can be ruled out as a possible explanation for this observation.

Ames Laboratory is operated for the US Department of Energy by Iowa State University under Contract W-7405-Eng-82. This work was supported by the Office of Biological and Environmental Research. T. Reinot was supported by the Solid State Chemistry and Polymers Program of the National Science Foundation (Grant DMR-9908714).

REFERENCES

Ali, S. H., and J. A. DeCaprio. 2001. Cellular transformation by SV40 large T antigen: interaction with host proteins. *Semin. Cancer Biol.* 11:15–23.

Auersperg, N., S. L. Maines-Bandiera, H. G. Dyck, and P. A. Kruk. 1994. Characterization of cultured human ovarian surface epithelial cells: phenotypic plasticity and premalignant changes. *Lab. Invest.* 71:510–518.

Chen, L. B., I. C. Summerhayes, L. V. Johnson, M. L. Walsh, S. D. Bernal, and T. J. Lampidis. 1982. Probing mitochondria in living cells with rhodamine 123. *Cold Spring Harb. Symp. Quant. Biol.* 46:141–155.

Chou, J. Y. 1989. Differentiated mammalian cell lines immortalized by temperature-sensitive tumor viruses. *Mol. Endocrinol.* 3:1511–1514.

Conover, C. A., L. C. Hartmann, S. Bradley, P. Stalboerger, G. G. Klee, K. R. Kalli, and R. B. Jenkins. 1998. Biological characterization of human epithelial ovarian carcinoma cells in primary culture: the insulin-like growth factor system. *Exp. Cell Res.* 238:439–449.

Dairkee, S. H., and A. J. Hackett. 1991. Differential retention of rhodamine 123 by breast carcinoma and normal human mammary tissue. *Breast Cancer Res. Treat.* 18:57–61.

Davis, S., M. J. Weiss, J. R. Wong, T. J. Lampidis, and L. B. Chen. 1985. Mitochondrial and plasma membrane potentials cause unusual accumulation and retention of rhodamine 123 by human breast adenocarcinoma-derived MCF-7 cells. *J. Biol. Chem.* 260:13844–13850.

Furusawa, A., T. Suga, and U. Kiyoshi. 1994. Photon echo spectroscopy on biological systems. I. Application to tissues. *J. Opt. Soc. Am. B.* 11: 1456–1461.

Hayes, J. M., T. Reinot, and G. J. Small. 1999. Hole burning properties of aluminum phthalocyanine tetrasulphonate in water-containing poly (2-hydroxyethyl methacrylate) films. *Chem. Phys. Lett.* 312:362–368.

Hayes, J. M., and G. J. Small. 1978. Non-photochemical hole burning and impurity site relaxation processes in organic glasses. *Chem. Phys.* 27:151–157.

Jankowiak, R., J. M. Hayes, and G. J. Small. 1993. Spectral hole-burning spectroscopy in amorphous molecular solids and proteins. *Chem. Rev.* 93:1471–1502.

Jenkins, N., editor. 1999. Animal Cell Biotechnology: Methods and Protocols. Humana Press, Totowa, New Jersey.

Jha, K. K., S. Banga, V. Palejwala, and H. L. Ozer. 1998. SV40-mediated immortalization. *Exp. Cell Res.* 245:1–7.

Johnson, L. V., M. L. Walsh, and L. B. Chen. 1980. Localization of mitochondria in living cells with rhodamine 123. *Proc. Natl. Acad. Sci. USA.* 77:990–994.

Kador, L., D. Haarer, and R. Personov. 1987a. Stark effect of polar and unpolar dye molecules in amorphous hosts, studied via persistent spectral hole burning. *J. Chem. Phys.* 86:5300–5307.

Kador, L., R. Personov, W. Richter, T. Sesselmann, and D. Haarer. 1987b. Laser photochemistry and hole burning spectroscopy in polymers and glasses: external field effects. *Polymer J.* 19:61–71.

Kalli, K. R., O. I. Falowo, L. K. Bale, M. A. Zshunke, P. C. Roche, and C. A. Conover. 2002. Functional insulin receptors on human epithelial ovarian carcinoma cells: implications for IGF-II mitogenic signalling. *Endocrinology.* 143:3259–3267.

Kenney, M. J., R. Jankowiak, and G. J. Small. 1990. Dispersive kinetics of nonphotochemical hole growth for oxazine 720 in glycerol, poly(vinyl alcohol) and their deuterated analogs. *Chem. Phys.* 146:47–61.

Kim, W. H., T. Reinot, J. M. Hayes, and G. J. Small. 1996. Non-photochemical hole burning in hyperquenched glassy films of water: a pronounced deuteration effect. *J. Chem. Phys.* 104:6415–6417.

Maines-Bandiera, S. L., P. A. Kruk, and N. Auersperg. 1992. Simian virus 40-transformed human ovarian surface epithelial cells escape normal growth controls but retain morphogenetic responses to extracellular matrix. *Am. J. Obstet. Gynecol.* 167:729–735.

Milanovich, N., M. Rätsep, T. Reinot, J. M. Hayes, and G. J. Small. 1998a. Stark hole burning of aluminum phthalocyanine tetrasulfonate in normal and cancer cells. *J. Phys. Chem. B.* 102:4265–4268.

Milanovich, N., T. Reinot, J. M. Hayes, and G. J. Small. 1998b. Aluminum phthalocyanine tetrasulfonate in MCF-10F, human breast epithelial cells: a hole burning study. *Biophys. J.* 74:2680–2688.

Modica-Napolitano, J. S., and J. R. Aprille. 1987. Basis for the selective cytotoxicity of rhodamine 123. *Cancer Res.* 47:4361–4365.

Nitta, M., H. Katabuchi, H. Ohtake, H. Tashiro, M. Yamaizumi, and H. Okamura. 2001. Characterization and tumorigenicity of human ovarian surface epithelial cells immortalized by SV40 large T antigen. *Gynecol. Oncol.* 81:10–17.

Rätsep, M., T. W. Johnson, P. R. Chitnis, and G. J. Small. 2000. The red-absorbing chlorophyll-a antenna states of photosystem. I: A hole-burning study of *Synechocystis* sp. PCC 6803 and its mutants. *J. Phys. Chem. B.* 104:836–847.

Rätsep, M., H. M. Wu, J. M. Hayes, R. E. Blankenship, R. J. Cogdell, and G. J. Small. 1998a. Stark hole-burning studies of three photosynthetic complexes. *J. Phys. Chem. B.* 102:4035–4044.

Rätsep, M., H. M. Wu, J. M. Hayes, and G. J. Small. 1998b. Stark hole-burning spectroscopy of a photosynthetic complex: LH2 of purple bacteria. *Spectrochim. Acta. Part A.* 54A:1279–1289.

Reddy, N. R. S., S. V. Kolaczkowski, and G. J. Small. 1993. A photoinduced persistent structural transformation of the special pair of a bacterial reaction center. *Science.* 260:68–71.

Reinot, T., J. M. Hayes, and G. J. Small. 1997a. Electronic dephasing and electron-phonon coupling of aluminum phthalocyanine tetrasulfonate in hyperquenched and annealed glassy films of ethanol and methanol over a broad temperature range. *J. Chem. Phys.* 106:457–466.

Reinot, T., J. M. Hayes, and G. J. Small. 1999. Laser-induced hole filling and spectral diffusion of aluminum phthalocyanine tetrasulfonate in hyperquenched glassy films. *J. Chem. Phys.* 110:4820–4827.

Reinot, T., J. M. Hayes, and G. J. Small. 2000. Fundamentals of nonphotochemical hole burning spectroscopy and application to complex systems. *Photon. Sci. News.* 6:83–99.

Reinot, T., W. H. Kim, J. M. Hayes, and G. J. Small. 1997b. New standard for high-temperature persistent-hole-burning molecular materials: aluminum phthalocyanine tetrasulfonate in buffered hyperquenched glassy films of water. *J. Opt. Soc. Am. B.* 14:602–608.

Reinot, T., and G. J. Small. 2000. Modeling of dispersive nonphotochemical hole growth kinetics data: Al-phthalocyanine tetrasulphonate in hyperquenched glassy water. *J. Chem. Phys.* 113:10207–10214.

Reinot, T., and G. J. Small. 2001. Non-Lorentzian zero-phonon holes and new insights on nonphotochemical hole burning: Al-phthalocyanine in hyperquenched glassy water. *J. Chem. Phys.* 114:9105–9114.

Reinot, T., V. Zazubovich, J. M. Hayes, and G. J. Small. 2001. New insights on persistent nonphotochemical hole burning and its application to photosynthetic complexes. *J. Phys. Chem. B.* 105:5083–5098.

Resnick-Silverman, L., Z. Pang, G. Li, K. K. Jha, and H. L. Ozer. 1991. Retinoblastoma protein and simian virus 40-dependent immortalization of human fibroblasts. *J. Virol.* 65:2845–2852.

Sakanoue, J., K. Ichikawa, Y. Nomura, and M. Tamura. 1997. Rhodamine 800 as a probe of energization of cells and tissues in the near-infrared region: a study with isolated rat liver mitochondria and hepatocytes. *J. Biochem. (Tokyo).* 121:29–37.

Scully, R. E. 1977. Ovarian tumors. *Am. J. Pathol.* 87:686–720.

Shu, L., and G. J. Small. 1992. Mechanism of nonphotochemical hole burning: cresyl violet in polyvinyl alcohol films. *J. Opt. Soc. Am. B.* 9:724–732.

Silbey, R. J., J. M. A. Koedijk, and S. Völker. 1996. Time and temperature dependence of optical linewidths in glasses at low temperature. *J. Chem. Phys.* 105:901–909.

Summerhayes, I. C., T. J. Lampidis, S. D. Bernal, J. J. Nadakavukaren, K. K. Nadakavukaren, E. L. Shepherd, and L. B. Chen. 1982. Unusual retention of rhodamine 123 by mitochondria in muscle and carcinoma cells. *Proc. Natl. Acad. Sci. USA.* 79:5292–5296.

Van den Berg, R., and S. Völker. 1988. Site-selection spectroscopy and hole-burning of ionic dyes in amorphous hosts at low temperature. *Chem. Phys.* 128:257–273.

Walsh, C. A., M. Berg, L. R. Narasimhan, and M. D. Fayer. 1987. A picosecond photon echo study of a chromophore in an organic glass: temperature dependence and comparison to nonphotochemical hole burning. *J. Chem. Phys.* 86:77–87.

Walsh, R. J. 2002. Nonphotochemical hole-burning imaging studies of in vitro carcinoma and normal cells utilizing a mitochondrial specific dye. Ph.D. thesis. Iowa State University, Ames, Iowa. 140 pp.

Walsh, R. J., T. Reinot, J. M. Hayes, K. R. Kalli, L. C. Hartmann, and G. J. Small. 2002. Nonphotochemical hole burning spectroscopy of a mitochondrial selective rhodamine dye molecule in normal and cancerous ovarian surface epithelial cells. *J. Lumin.* 98:115–121.

Wu, H. M., M. Rätsep, C. S. Young, R. Jankowiak, R. E. Blankenship, and G. J. Small. 2000. High-pressure and stark hole-burning studies of chlorosome antennas from *Chlorobium tepidum*. *Biophys. J.* 79:1561–1572.

Zazubovich, V., S. Matsuzaki, T. W. Johnson, J. M. Hayes, P. R. Chitnis, and G. J. Small. 2002. Red antenna states of photosystem I from *cyanobacterium Synechococcus elongatus*: a spectral hole burning study. *Chem. Phys.* 275:47–59.